EDGE ARTICLE

Check for updates

An implantable ionic liquid-gel microelectrode for *in vivo* monitoring of K^{+} levels in the living rat brain†

Zhihui Zhang, Zehui Chen, Tao Liu* and Limin Zhang [ID] *

The exploration of new interfaces for *in vivo* analysis holds great promise for electrochemical acquisition of chemical signals involved in brain events. In this study, we designed and created an implantable electrode using a liquid/liquid (L/L) interface concept to monitor *in vivo* variations of K^{+} in the living brain. Poly(1-butyl-3-vinylimidazolium bis(trifluoro-methylsulfonyl)imide) (PB) and an ionic liquid of 1-decyl-3-methylimidazolium bis(trifluoromethanesulfonyl)-imide ($C_{10}M$) were optimized to form a uniform ionic liquid gel (ILG), which exhibits a wide potential window and remarkably enhances interfacial mechanical stability. Furthermore, the specific ionophore [2.2.3]-triazacryptand (TAC) was optimized and incorporated into the ILG (ILG-TAC) to molecularly tailor the micro-interface between the gel phase and water phase. The developed implantable ILG-TAC electrode demonstrated high selectivity for K^{+}, and good anti-biofouling capability with a signal deviation less than 8.5% over 50 days of continuous implantation. This ion-transfer-based sensing strategy introduces a novel approach for *in vivo* analysis, especially beneficial for detecting redox inactive species.

Introduction

The electrochemical technique using implantable microelectrodes has emerged as a pivotal and promising approach for acquiring *in vivo* chemical signals in the brain, aiding in the exploration of molecular mechanisms underlying brain events.[1,2] Widely used sensing strategies rely on solid electrode/electrolyte interfaces, such as carbon fiber and noble-metal microelectrodes, which generate faradaic current signals *via* electron transfer processes.[3–6] Nonetheless, these sensing models frequently encounter limitations in detecting electrochemically inactive species, as these species are incapable of undergoing redox reactions within the water-splitting potential window.[6]

The interface between two immiscible electrolyte solutions, referred to as the liquid/liquid (L/L) interface supported by a pipette, offers significant advantages for the direct analysis of ionic species.[7–10] This interface operates based on the difference in solvation energies of ions in two adjacent phases, generating ionic current signals and characteristic transfer potentials for discrimination.[11–14] Unlike conventional electrochemical sensors, L/L interfacial systems depend on ion transfer rather than electron transfer, enabling the identification and

quantification of non-electroactive species. Moreover, the L/L interface supported by a pipette allows for high spatial resolution for *in vivo* analysis by reducing the tip size to the micrometer scale.[15–19] Despite its conceptual robustness, the application of the L/L interface for *in vivo* analysis is still in its early stages.[16,20] For instance, Zhang *et al.* employed a 1,2-dichloroethane (1,2-DCE)/water interface sensor to detect choline in the brain, demonstrating its potential feasibility for *in vivo* analysis.[21] However, the inherent mechanical instability of the L/L interface often poses a risk of organic solvent leakage, which can induce biological toxicity and impair brain function.[22] To address this, Gu *et al.* recently developed an enhanced L/L interfacial iontronics by using polyvinylchloride (PVC) to improve the interfacial stability of the organic phase.[23] A potential shortcoming is that the low conductivity of PVC may increase the resistance of the organic phase, resulting in elevated background current signals.[22,24] Additionally, in the complex brain environment where numerous ionic interferences coexist,[25] the analytical model solely based on the inherent ion transfer potentials at the L/L interface faces significant limitations.

Motivated by these challenges, we designed and developed an implantable L/L interfacial sensor supported by a micropipette filled with an ionic liquid-gel (ILG) for *in vivo* monitoring of extracellular K^{+} in the living rat brain (Scheme 1). A hydrophobic ionic liquid, 1-decyl-3-methylimidazolium bis(trifluoromethanesulfonyl)imide ($C_{10}M$), was optimized as the organic phase. Simultaneously, conductive poly(1-butyl-3-vinylimidazolium bis(trifluoro-methylsulfonyl)imide) (PB),

Department of Chemistry, School of Chemistry and Molecular Engineering, East China Normal University, Dongchuan Road 500, Shanghai 200241, China. E-mail: lmzhang@chem.ecnu.edu.cn; taoliu@chem.ecnu.edu.cn
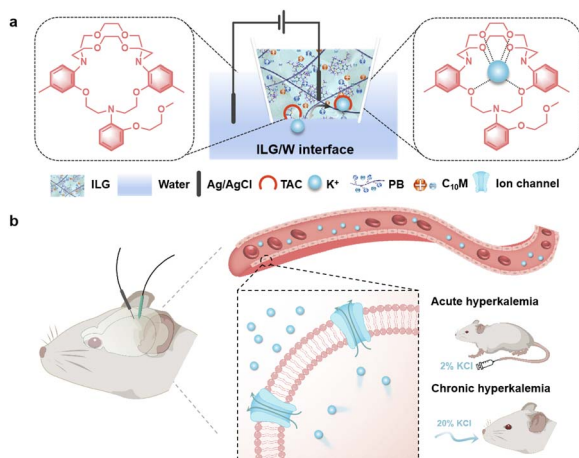
Scheme 1 (a) Working principle of the molecularly tailored ILG-TAC/W interface supported by a micropipette for facilitating the K$^+$ transfer process. (b) *In vivo* determination of K$^+$ in the living rat brain with acute and chronic hyperkalemia models using the developed ILG-TAC electrode.

instead of PVC, was used to enhance the mechanical stability of the C$_{10}$M/W interface by forming an organic gel. It is important to note that the traditional L/L interfaces require the addition of an organic supporting electrolyte at relatively high concentrations ($\sim10^{-3}$ M to 10^{-2} M) to ensure sufficient electrical conductivity of the organic phase.[13] The use of conductive ILs as the organic phase eliminates the requirement for supplementary organic supporting electrolytes, thus simplifying the fabrication process of interfacial sensors. By molecularly tailoring the ILG/water interface using the specific K$^+$ ionophore, [2.2.3]-triazacryptand (TAC)(ILG-TAC/W), we achieved selective facilitation of K$^+$ transfer from the aqueous phase to the ILG phase. The developed ILG-TAC electrode exhibited remarkable anti-fouling capability, maintaining a current signal decrease of less than 8.5% even after 50 days of immersion in bovine serum albumin solution. Eventually, the resulting ILG-TAC/W interfacial sensor was successfully implanted into the cerebral cortex of rat brains, and *in vivo* variation of K$^+$ in rat brains was selectively determined with hyperkalemia models.

Results and discussion

The ionophores of [2.2.3]-triazacryptand (TAC), C2, and dibenzo-18-crown-6 (C3, a commonly used ionophore towards K$^+$) were taken as specific recognition molecules for K$^+$. Among them, TAC and C2 were synthesized as reported previously (Scheme S1, ESI†),[26,27] and characterized by ^{1}H NMR and ^{13}C NMR spectroscopy (Fig. S1†). Moreover, PB was prepared and characterized by ^{1}H NMR and FT-IR spectroscopy (Fig. S2†).[28] The primary criterion for selecting the IL was its high hydrophobicity, as this property enables the formation of a well-separated L/L interface with aqueous solution. We selected three hydrophobic ILs with the bis(trifluoromethanesulfonyl) imide anion, 1-ethyl-3-methylimidazolium bis(trifluoromethyl-sulfonyl)imide (C$_2$M), 1-butyl-3-methylimidazolium

bis(trifluoromethyl-sulfonyl)-imide (C$_4$M), and 1-decyl-3-methylimidazolium bis(trifluoromethanesulfonyl)imide (C$_{10}$M) as the organic phase to form C$_2$M/W, C$_4$M/W, and C$_{10}$M/W interfaces with aqueous solution, respectively. The C$_{10}$M/W micro-interface exhibited the widest polarized potential window (~800 mV) as determined by cyclic voltammetry (CV) (Fig. S3†), and hence was chosen to fabricate the uniform ILG with PB at the mass ratio of 1:1 (Fig. 1a and b). When the pipette filled with ILG was left standing vertically for 30 min, the ILG level within the pipette showed no noticeable change (Fig. 1d). In contrast, the liquid level of pure C$_{10}$M in the pipette moved about 5 mm within 10 s, resulting in droplet formation at the pipette tip (Fig. 1c). These results indicate that the incorporation of PB efficiently enhanced the mechanical stability of the ILG interface, which is critical for subsequent implantation testing in the brain. Then, the micropipette was prepared and characterized by scanning electron microscopy (SEM), exhibiting a round orifice with a radius of ~2.5 μm (Fig. 1e(i)). The ionophore of TAC was dissolved in the organic gel to tailor the ILG/W micro-interface for K$^+$ detection *via* specific chemical binding. In order to ensure the position of the L/L interface, fluorescein was added to the gel phase. As shown in Fig. S4,† the fluorescence signal was clearly observed along the micropipette, indicating that the gel filled the micropipette uniformly. Furthermore, the ILG-TAC was further demonstrated to completely fill the micropipette tip by microscopy (Fig. 1e(ii)). The polarized potential window remained almost unchanged after TAC was incorporated into ILG in blank aqueous solution, indicating that the addition of TAC had negligible effect on the initial potential window (Fig. 1f).

To verify the K$^+$ recognition capability of the ILG-TAC/W interface, the voltammetric behaviors were recorded using electrochemical cells 1–2. As illustrated in Fig. 1g, a well-defined positive current with a half-wave potential of ~0.26 V was observed at the ILG-TAC electrode in aqueous solution containing 5 mM K$^+$ (curve i), while no significant current response was observed at the ILG/W interface, even though the K$^+$ concentration was enhanced to 80 mM (curve iv). Thus, such current response at the ILG-TAC electrode was ascribed to the transfer of K$^+$ facilitated by TAC. The transfer potentials of facilitated ion transfer were calibrated using the tetramethylammonium cation (TMA$^+$) as an internal reference ion. In this case, the amount of TAC (200 mM) exceeds that of K$^+$, making the diffusion of K$^+$ the rate-determining step of facilitated ion transfer. The forward steady-state wave seen in the voltammetric curve is controlled by the hemispherical diffusion of K$^+$ from the aqueous phase to the ILG-TAC phase by the following chemical reaction:

$$K^+ (W) + TAC (ILG) \rightarrow K\text{-}TAC^+ (ILG)$$

During the reverse scan, the voltammetric curve indicates the hemispherical diffusion of the [K-TAC]$^+$ complex away from the ILG-TAC/W interface. From a thermodynamic perspective, the half-wave potential ($\Delta_o^w \phi_{1/2}$) for the reaction between K$^+$ and TAC in the case of a 1:1 ($n = 1$) mass ratio can be expressed as:
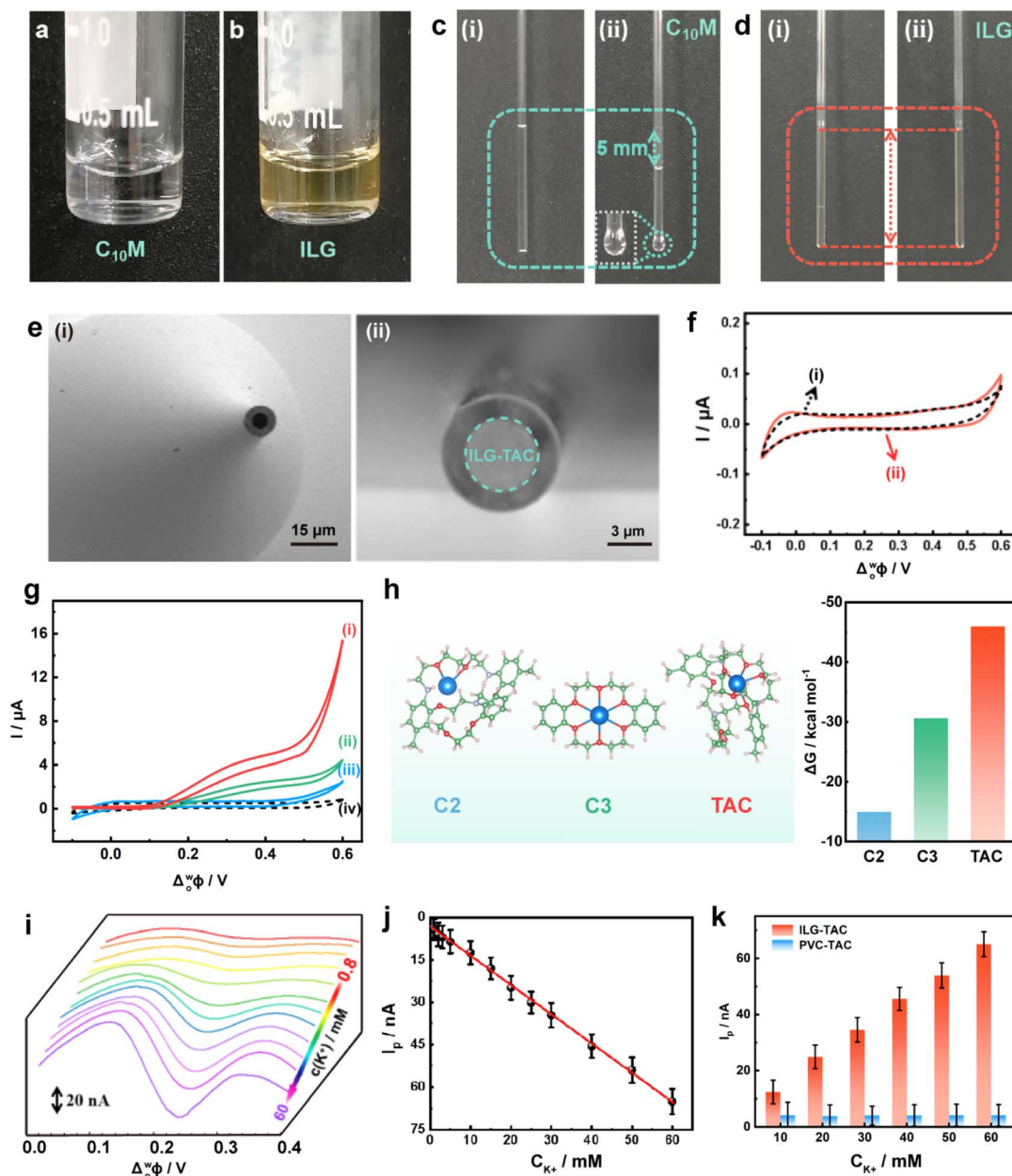
Fig. 1 (a and b) Typical photographs of $C_{10}M$ and ILG formed by $C_{10}M$ and PB. (c and d) (i) Upright and (ii) inverted positions of $C_{10}M$ and ILG in a pipette. (e) (i) SEM image of a micropipette, and (ii) confocal image of the micropipette filled with ILG-TAC. (f) CV curves of ILG (i) and ILG-TAC (ii) electrodes using cell 1: Ag|AgCl|ILG||5 mM NaCl|AgCl|Ag. (g) CV curves recorded at the three ionophores tailored ILG/W micro-interface ((i) ILG-TAC/W, (ii) ILG-C3/W, (iii) ILG-C2/W and (iv) ILG/W) using electrochemical cell 2: Ag|AgCl|ILG + TAC||x mM K^+|AgCl|Ag ((i–iii) $x = 5$; (iv) $x = 80$), scan rate: 10 mV s^{-1}. (h) Gibbs free energies of the complexation reaction between C2, C3 and TAC and K^+ obtained by DFT simulations. (i) DPV curves obtained at the ILG-TAC electrode in the presence of different K^+ concentrations (C_{K+}: 0, 0.8, 1, 2, 5, 10, 15, 20, 25, 30, 40, 50 and 60 mM). (j) I_p values obtained at the ILG-TAC electrode at different K^+ concentration. (k) Comparison of I_p values at the ILG-TAC and the PVC-TAC electrodes under different K^+ concentrations.

$$\Delta_o^w \phi_{1/2} = \Delta_o^w \phi_{K^+}^{0'} + \frac{RT}{zF} \ln(\beta_{TAC}[K^+])$$

where $\Delta_o^w \phi_{K^+}^{0'}$ represents the formal potential of K^+ transfer across the ILG/W interface, z denotes the transferred charge of K^+, β_{TAC} is the association constant in the ILG phase, and $[K^+]$ indicates the concentration of K^+ in the aqueous phase. Moreover, the electrochemical performance of the ILG-TAC is less affected by the silanization of the micropipette (Fig. S5†). By

comparison, a lower current response was observed at more positive $\Delta_o^w \phi_{1/2}$ (~0.31 V) when using C3 as ionophore in ILG (ILG-C3), but no obvious current response was obtained at the C2 tailored ILG/W interface (ILG-C2/W) (curves ii–iii, Fig. 1g). These results suggested that TAC is a suitable ionophore to facilitate the transfer of K^+ at the ILG-TAC/W interface. Upon incorporating the ionophore into the ILG, density functional theory (DFT) calculations were performed to estimate the Gibbs

free energy (ΔG) values of three ionophores reacted with K$^+$. As shown in Fig. 1h, the ΔGs of TAC, C2, and C3 were ~-46.0 kcal mol^{-1}, ~-15.0 kcal mol^{-1}, and ~-30.6 kcal mol^{-1}, respectively. The most negative binding energy of TAC suggests that it has a stronger binding affinity with K$^+$ than C2 and C3. Furthermore, the molecular cavity size of TAC is estimated to be 2.90 Å, which aligns more closely with the ionic diameter of K$^+$ (~2.66 Å) than those of C2 (~4.32 Å) and C3 (~3.2 Å). Coupled with additional oxygen binding sites in TAC, the selective facilitation of K$^+$ transfer was achieved at the ILC-TAC/W interface. By testing the transfer current at the ILG-TAC/W interface over different times, 4 min was optimized as the reaction time for K$^+$ determination (Fig. S6†). Owing to the high sensitivity, differential pulse voltammetry (DPV) was conducted to study the variation of current responses in the aqueous phase containing different concentrations of K$^+$. The peak current (I_p)
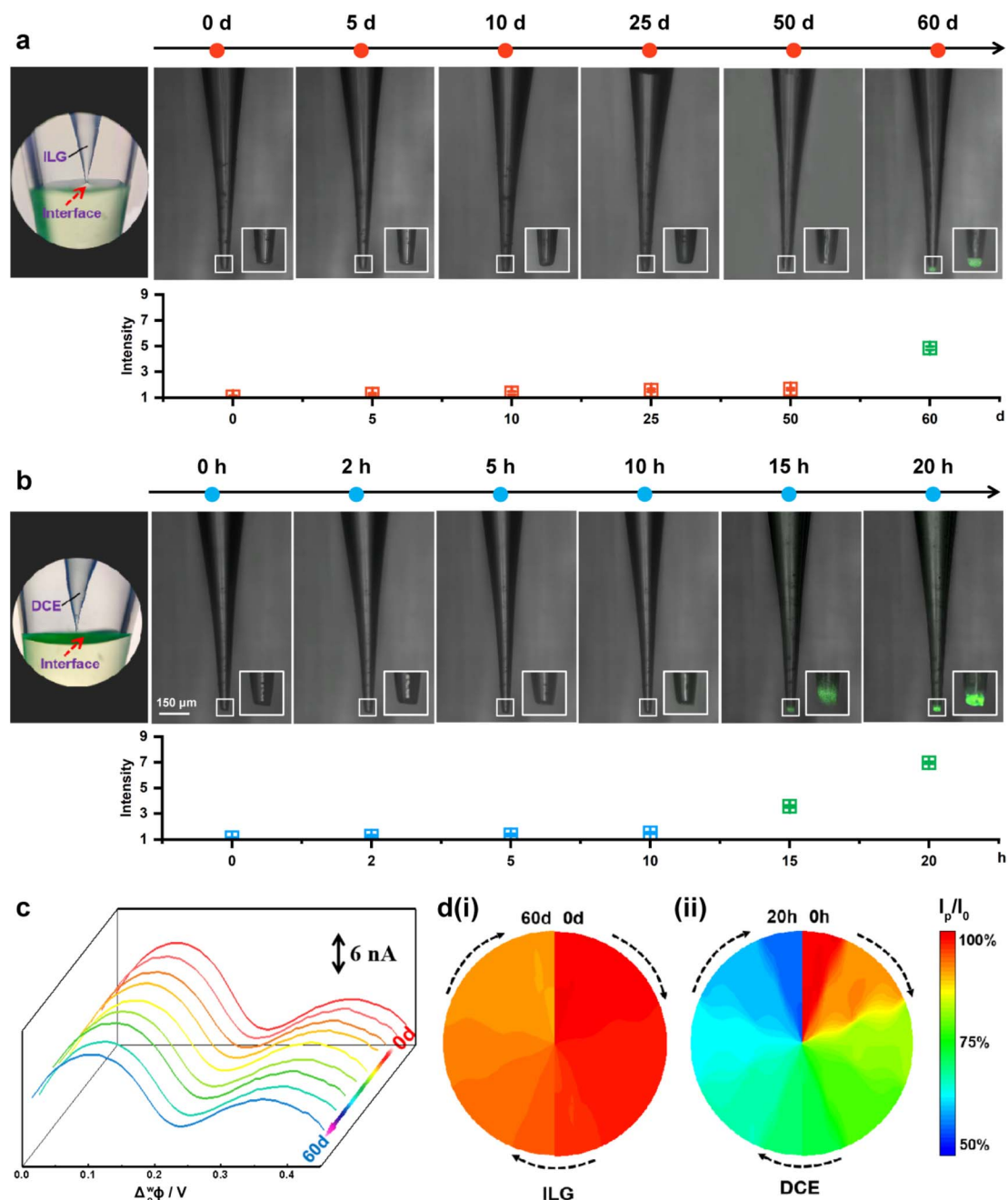

Fig. 2 (a) Fluorescence images (upper) and relative fluorescence intensity (lower) tested at the ILG-TAC electrode immersed in 5 mg per mL FITC–BSA solution for 0 d, 5 d, 10 d, 25 d, 50 d and 60 d. (b) Fluorescence images (upper) and relative fluorescence intensity (lower) obtained at the micropipette filled with 1,2-DCE which was immersed in 5 mg per mL FITC–BSA solution for 0 h, 2 h, 5 h, 10 h, 15 h and 20 h. (c) DPV curves of the ILG-TAC electrode for 5 mM K$^+$ after immersion in 5 mg per mL BSA for 0 to 60 d. (d) I_p/I_0 variations at the ILG-TAC electrode during immersion in BSA for 60 days (i). I_p/I_0 at a micropipette filled with 1,2-DCE during immersion in BSA for 20 hours (ii). I_0 represents the initial peak current obtained at the ILG-TAC electrode.

increased with increasing K^+ concentration, exhibiting a linear relationship ranging from 0.8 to 60 mM, with a detection limit of 0.13 mM (Fig. 1i and j). Moreover, the mass ratio of $C_{10}M$ to PB was changed to 1 : 2 and 2 : 1, but the much narrower linear range was obtained under these conditions (Fig. S7†). As a result, the 1 : 1 mass ratio of $C_{10}M$ to PB was optimized to prepare the organic phase for K^+ determination. In fact, a popular approach to overcome the L/L interfacial stability is using polyvinyl chloride (PVC) as a gelling agent to solidify the organic phase.[29,30] We incorporated PVC into the 1,2-DCE phase with TAC, resulting in a PVC-TAC gel electrode. The electrochemical behavior of the PVC-TAC electrode was studied by DPV (Fig. S8†). The same amount of K^+ was found to generate a lower current response at the PVC-TAC microelectrode than the ILG-TAC microelectrode (Fig. 1k). These observations indicate that the ILG-TAC electrodes possess a wider linear range and higher sensitivity to K^+.

Electrochemical detection of chemical substances in the complex biological brain environment is widely used for the early diagnosis, prevention and treatment of diseases.[31–33] However, a significant challenge in electrochemical sensing based on the current output arises when coexisting species (*e.g.* biomacromolecules and proteins) nonspecifically adsorb onto the polarized interface, resulting in the loss of current

signals.[34–36] Therefore, the anti-biofouling capability of the developed ILG-TAC/W interface is crucial for reliable *in vivo* analysis. Bovine serum albumin (BSA) was selected as a model protein to simulate the surface biofouling in rat brains.[27,37] Surprisingly, no obvious fluorescence was observed at the interface after the ILG-TAC electrode was immersed in the fluorescein isothiocyanate(FITC)-labeled BSA (FITC-BSA) solution for 50 days (Fig. 2a). Moreover, the peak current exhibited a decrease of less than 8.5% (Fig. 2c and d(i)). Nevertheless, fluorescence was clearly observed at the 1,2-DCE/W interface supported by a micropipette after immersion in BSA solution for 15 h (Fig. 2b). Meanwhile, the current response to K^+ was rapidly decreased by 44% (Fig. 2d(ii)). These results demonstrate that the ILG-TAC electrodes possess high anti-biofouling capability, suitable for *in vivo* analysis in the brain.

Selectivity is another important factor for *in vivo* analysis in the practical brain environment. To assess the selective detection capability of the ILG-TAC microelectrode for K^+, selectivity tests were conducted against metal ions, anions, amino acids, and biological species that coexist in the rat brain. The amount of interference is decided referring to their concentrations in the practical brain as reported previously.[11,12] Na^+ and Ca^{2+} are identified as the main interferences due to their similar transfer potentials to that of K^+ and high concentrations in the brain
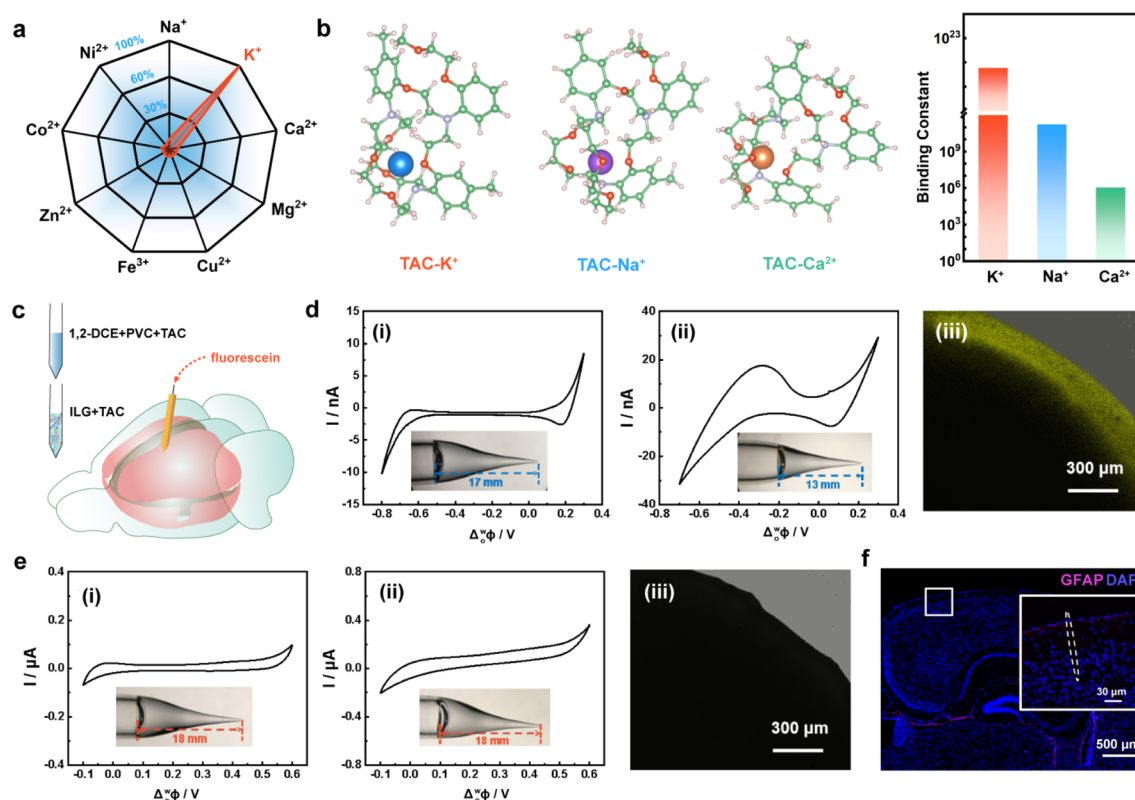

Fig. 3 (a) Selectivity tests of the ILG-TAC electrode for metal anions (Na^+, Ca^{2+}, Mg^{2+}, Cu^{2+}, Fe^{3+}, Zn^{2+}, Co^{2+}, and Ni^{2+} at concentrations of 10 mM for Na^+, 1 mM for Ca^{2+} and Mg^{2+}, and 10 μM for other ions). (b) Binding constants between TAC and K^+, Na^+ and Ca^{2+} obtained from DFT simulations. (c) A schematic diagram of the implantation of the 1, 2-DCE-TAC electrode and ILG-TAC electrode filled with fluorescein in rat brains. (d and e) Typical CV curves obtained at the 1,2-DCE-TAC electrode (d) and ILG-TAC electrode (e) in aCSF solution before (i) and after (ii) implantation in the rat brain for 20 min. The fluorescence image of brain slices after implantation of the electrode for 5 h (iii). (Inset) Photographs of the interfaces filled in capillaries under conditions of (d) and (e), respectively. (f) GFAP staining images of coronal brain sections from the rat in the group implanted with the ILG-TAC electrode for 7 days.

(Na$^+$ at ~100 mM and Ca^{2+} at ~1 mM). As depicted in Fig. 3a, the interferences from Na$^+$ and Ca^{2+} were less than 5.7% and 4.5%, respectively. For other species, including anions, amino acids and biologically relevant reagents, the interference was also negligible (<4.1%) (Fig. S9†). Moreover, slight changes (<6.1%) were observed in competition tests for K$^+$ in the presence of other interferences (Fig. S10†), indicating a high selectivity of the ILG-TAC microelectrode for the detection of K$^+$. DFT simulations further estimated the binding constant of TAC with K$^+$ to be 5.8×10^{21}, which is 3.4×10^{10} times greater than that of Na$^+$, and 5.3×10^{15} times greater than that of Ca^{2+} (Fig. 3b). This strong binding affinity of TAC with K$^+$ explains the high selectivity of the ILG-TAC electrode towards K$^+$.

The mechanical stability of the L/L interface supported by a micropipette is vital for *in vivo* acquisition of K$^+$ in the brain (Fig. 3c). To address this, PB, a polymer of ionic liquid, was incorporated into C$_{10}$M to fabricate gel microelectrodes. As expected, the ILG-TAC/W interface exhibited a stable polarized potential window even after being implanted in the brain for 24 h without obvious gel interfacial movement (Fig. 3e(i) and (ii)). At the same time, we added fluorescein in the gel phase to observe the moving of the gel interface. Once the organic gel flows out of the micropipette and contaminates the brain tissue, fluorescence signals will be observed on the brain slices. As displayed in Fig. 3e(iii), no fluorescence signal was observed in the brain slice, indicating no leakage of gel from the micropipette. These observations demonstrate that the ILG-TAC electrodes possess excellent interfacial stability, which is highly suitable for implantable determination. In contrast, the conventional 1,2-DCE/W interface supported by a micropipette

exhibited a significant change of polarized potential window after 20 min of implantation in the brain (Fig. 3d). The liquid level of 1,2-DCE in the micropipette also shifted toward the orifice, reducing the liquid length within the micropipette from 17 mm to 13 mm (Fig. 3d(i) and (ii)). Fluorescein was used to label the 1,2-DCE phase, and fluorescence was observed at the border of the brain slice using confocal microscopy, revealing the leakage of 1,2-DCE into the brain tissue (Fig. 3d(iii)).

After mechanical injury to the brain, astrocytes proliferate abnormally, leading to increased expression of glial fibrillary acidic protein (GFAP).[38] Thus, GFAP expression in the rat brain serves as a reliable indicator of tissue damage caused by implanted microelectrodes. To assess the inflammatory response induced by the implantation of the ILG-TAC microelectrodes, GFAP expression in the rat brain was evaluated. As displayed in Fig. 3f, only a little fluorescence response of GFAP expression was observed at the implantation site after 7 days compared to the initial situation (Fig. S11†). In combination with the results of 2,3,5-triphenyltetrazolium chloride (TTC) staining of brain tissue slices (Fig. S12†), the ILG-TAC microelectrodes demonstrated slight tissue damage and excellent biocompatibility *in vivo*. Therefore, the ILG-TAC electrode, with better mechanical stability and sensitivity for K$^+$, was established for implantable K$^+$ analysis in the brain.

In a state of hyperkalemia, the elevated potassium ion levels might interfere with the normal electrophysiological processes of neurons, leading to heightened neuronal excitability and potentially disrupting neural function[39,40] Based on the promising electrochemical performance, we implanted the ILG-TAC microelectrodes in the cerebral cortex to *in vivo* track K$^+$ in rat brains
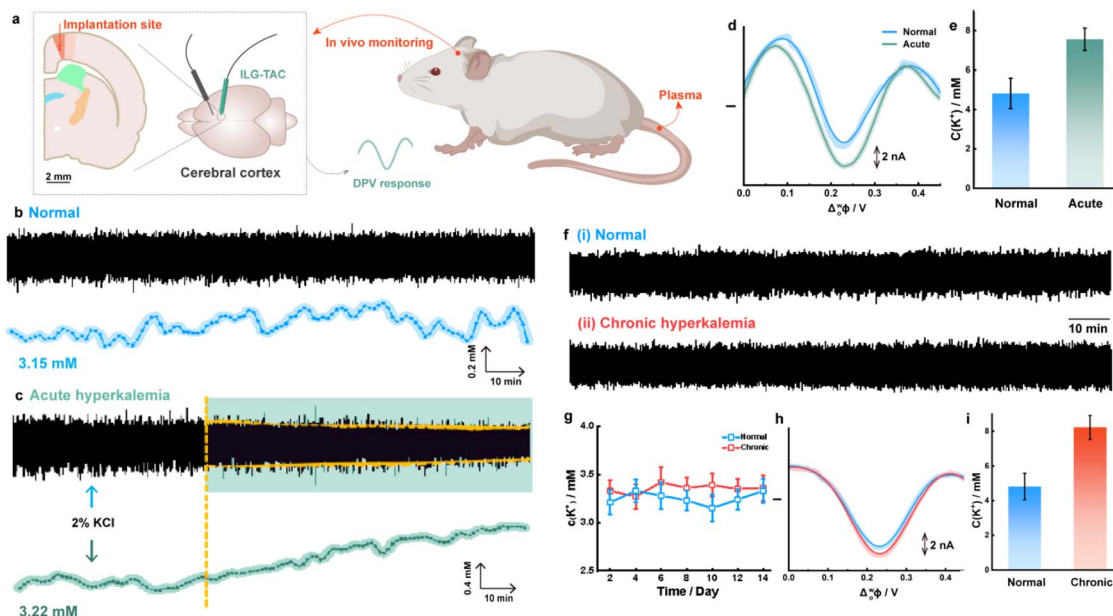

Fig. 4   (a) Schematic diagram of the ILG-TAC electrode implanted in the cerebral cortex for *in vivo* detection of K$^+$. (b and c) LFP recording (upper) and *in vivo* measurements of K$^+$ levels (lower) in (b) normal and (c) acute hyperkalemia rat brains. (d) DPV curves of the ILG-TAC electrode in the cortex of normal and acute hyperkalemia rats. (e) The concentrations of K$^+$ in the plasma of normal and acute hyperkalemia rats. (f) LFP recording in (i) normal and (ii) chronic hyperkalemia rats. (g) *In vivo* measurements of K$^+$ levels in the cortex of the rat brain with chronic hyperkalemia for 14 days. (h) DPV curves of the ILG-TAC electrode in the cortex of normal and chronic hyperkalemia rats. (i) The concentrations of K$^+$ in the plasma of normal and chronic hyperkalemia rats.

(Fig. 4a). In this study, acute and chronic hyperkalemia models were constructed. We constructed a rat model of acute hyperkalemia by continuous tail vein infusion of saline containing 2% KCl. Compared to the electrocardiogram (ECG) of normal rats, the QRS complex peak voltage in the ECG of acute hyperkalemia model rats sharply decreased from 0.78 mV to 0.37 mV, while the peak voltage of the T-wave increased from 0.19 mV to 0.54 mV (Fig. S13†). This significant rise in T-wave amplitude is indicative of the severe electrolyte imbalance associated with acute hyperkalemia. The plasma K^+ concentration in the acute hyperkalemia model rats was further measured using the ILG-TAC microelectrode. The current response was found to be greater in the brain of an acute hyperkalemia rat compared to that of a normal rat (Fig. 4d), indicating that the plasma K^+ concentration in the terminal blood increased from 4.82 mM to 7.56 mM (Fig. 4e). These results indicate that the acute hyperkalemia model rats were successfully established. Subsequently, we used the ILG-TAC microelectrodes to track the K^+ concentration in rat brains. After stopping the injection of 2% KCl solution for 35 min, the K^+ concentration in the cerebral cortex began to rise slowly, increasing by approximately 23.6% within one hour (Fig. 4c). Simultaneously, we recorded local field potential (LFP) signals from the brains of acute hyperkalemia model rats. The intensity of neuronal LFP signals started to decrease significantly, which may be due to the increase in extracellular K^+ concentration leading to suppression of neuronal activity (Fig. 4c). In contrast, in control rats injected only with saline, there was no significant change in K^+ concentration in the cerebral cortex, and the corresponding LFP signals indicated that neuronal activity remained almost unchanged (Fig. 4b). These results suggest that the extracellular K^+ amount in the rat brain is susceptible to acute changes in plasma K^+ levels.[41,42]

On the other hand, the ILG-TAC microelectrode was employed to study the variations of K^+ levels in rat brains followed by chronic hyperkalemia. The chronic hyperkalemia model was achieved through unilateral nephrectomy and a diet supplemented with 20% KCl over a 14-day period. The ECG revealed a decrease in the QRS peak voltage from 0.78 to 0.49 mV (Fig. S14†). Additionally, peaked T-waves were observed in the ECG of chronic hyperkalemia rats, with the peak voltage increasing from 0.19 to 0.28 mV. Despite a 2.51 mM increase in plasma K^+ concentration in rats with chronic hyperkalemia (Fig. 4i), only minimal changes were noted in both cortical K^+ levels and spontaneous local field potential (LFP) activity (Fig. 4f–h). These results suggest that chronic alterations in plasma K^+ levels do not lead to significant fluctuations in K^+ concentrations within the brain. This regulatory mechanism may be mediated by adaptive modulation of K^+ influx or extrusion processes at the blood–brain barrier in response to chronic changes in plasma K^+ levels. However, it appears that the extent of such adaptive responses is markedly reduced during acute changes in plasma potassium.[43]

Conclusions

In summary, a novel ionic liquid gel electrode was designed and developed based on the principles of L/L electrochemistry. This innovative approach enables current measurements through an ion transfer mechanism, providing a promising platform for detecting various ionic species, including electrochemically inactive species. More importantly, the developed ILG electrode demonstrated remarkable interfacial stability and excellent anti-biofouling properties, both of which are critical for *in vivo* applications. Furthermore, the successful functionalization of the ILG electrode with specific ionophores for K^+ recognition significantly enhanced its selectivity. This advancement fulfills the stringent requirements for selective K^+ measurement in complex brain environments. These features allow the application of the L/L interface concept to implantable sensors within the real brain system. This study introduces a new strategy for the *in vivo* acquisition of chemical expressions within complex brain systems. It is worth noting that the present methodology can be easily extended to detect other chemical species, particularly non-electroactive ions, by incorporating appropriate ionophores into the organic phase. This flexibility not only broadens the applicability of the L/L electrode but also paves the way for future research in the field of biosensing and neurochemistry.

Ethical statement

All animal experiments were performed according to the guidelines of the Care and Use of Laboratory Animals formulated by the Ministry of Science and Technology of China and were approved by the Animal Care and Use Committee of East China Normal University (Shanghai, China).

Data availability

The authors confirm that the data supporting the findings of this study are available within the article and its ESI.†

Author contributions

L. M. Zhang and T. Liu conceived and designed the experiments, while Z. H. Zhang and Z. H. Chen performed the experiments and analyzed the data. All authors co-wrote the manuscript.

Conflicts of interest

There are no conflicts to declare.

Acknowledgements

Notes and references

1 X. Chai, X. Zhou, A. Zhu, L. Zhang, Y. Qin, G. Shi and Y. Tian, *Angew. Chem., Int. Ed.*, 2013, **52**, 8129–8133.

2 H. Dong, Q. Zhou, L. Zhang and Y. Tian, *Angew. Chem., Int. Ed.*, 2019, **5**, 13948–13953.

3 Y. Wang, Y. Qian, L. Zhang, Z. Zhang, S. Chen, J. Liu, X. He and Y. Tian, *J. Am. Chem. Soc.*, 2023, **145**, 2118–2126.

4 T. S. Davis, H. A. C. Wark, D. T. Hutchinson, D. J. Warren, K. O'Neill, T. Scheinblum, G. A. Clark, R. A. Normann and B. Greger, *J. Neural. Eng.*, 2016, **13**, 36001.

5 H. Wei, L. Li, J. Jin, F. Wu, P. Yu, F. Ma and L. Mao, *Anal. Chem.*, 2020, **14**, 10177–10182.

6 A. A. Muhammad, N. R. Logan, G. R. J. John and P. I. Pedro, *IEEE Trans. Neural Syst. Rehabil. Eng.*, 2019, **27**, 1724–1731.

7 D. Zhan, S. Mao, Q. Zhao, Z. Chen, H. Hu, P. Jing, M. Zhang, Z. Zhu and Y. Shao, *Anal. Chem.*, 2004, **76**, 4128–4136.

8 N. T. Iwai, M. Kramaric, D. Crabbe, Y. Wei, R. Chen and M. Shen, *Anal. Chem.*, 2018, **90**, 3067–3072.

9 S. Wilke, R. Schürz and H. Wang, *Anal. Chem.*, 2001, **73**, 1146–1154.

10 X. Huang, L. Xie, X. Lin and B. Su, *Anal. Chem.*, 2016, **88**, 6563–6569.

11 Q. Li, S. Xie, Z. Liang, X. Meng, S. Liu, H. H. Girault and Y. Shao, *Angew. Chem., Int. Ed.*, 2009, **48**, 8010–8013.

12 M. Welle, K. Alanis, M. L. Colombo, J. V. Sweedler and M. Shen, *Chem. Sci.*, 2018, **9**, 4937–4941.

13 P. J. Rodgers, P. Jing, Y. Kim and S. Amemiya, *J. Am. Chem. Soc.*, 2008, **130**, 7436–7442.

14 L. Xie, X. Huang and B. Su, *ACS Sens.*, 2017, **2**, 803–809.

15 M. L. Colombo, J. V. Sweedler and M. Shen, *Anal. Chem.*, 2015, **87**, 5095–5100.

16 S. Liu, Q. Li and Y. Shao, *Chem. Soc. Rev.*, 2011, **40**, 2236–2253.

17 P. He, Y. Shao, Z. Yu, X. Liang, J. Liu, Y. Bian, Z. Zhu, M. Li, C. M. Pereira and Y. Shao, *Anal. Chem.*, 2022, **94**, 9801–9810.

18 H. Wang, Y. Ruan, L. Zhu, X. Shi, W. Zhao, H. Chen and J. Xu, *Angew. Chem., Int. Ed.*, 2021, **133**, 13352–13358.

19 W. Ma, W. Xie, R. Tian, X. Zeng, L. Liang, C. Hou, D. Huo and D. Wang, *Sens. Actuators, B*, 2023, **377**, 133075.

20 S. H. Huang, M. Parandhaman, S. Farnia, J. Kim and S. Amemiya, *Chem. Commun.*, 2023, **59**, 9575–9590.

21 X. Wang, T. Xu, Y. Zhang, N. Gao, T. Feng, S. Wang and M. Zhang, *ACS Sens.*, 2021, **6**, 2757–2762.

22 J. D. Mann, A. B. Butler, J. E. Rosenthal, C. J. Maffeo, R. N. Johnson and N. H. Bass, *Ann. Neurol.*, 1978, **3**, 156–165.

23 C. Gu, F. Kong, S. Liang, X. Zhao, B. Kong, T. Jiang, J. Yu, Q. Li, Y. Lin, S. Bai and Y. Shao, *Sci. Adv.*, 2024, **10**, eadr7218.

24 C. Gu, X. Nie, J. Jiang, Z. Chen, Y. Dong, X. Zhang, J. Liu, Z. Yu, Z. Zhu, J. Liu, X. Liu and Y. Shao, *J. Am. Chem. Soc.*, 2019, **141**, 13212–13221.

25 L. Zhang and Y. Tian, *Acc. Chem. Res.*, 2018, **51**, 688–696.

26 H. He, M. A. Mortellaro, M. J. P. Leiner, R. J. Fraatz and J. K. Tusa, *J. Am. Chem. Soc.*, 2003, **125**, 1468–1469.

27 F. Zhao, Y. Liu, H. Dong, S. Feng, G. Shi, L. Lin and Y. Tian, *Angew. Chem., Int. Ed.*, 2020, **59**, 10426–10430.

28 J. Zhao, X. Shen, F. Yan, L. Qiu, S. Leec and B. Sun, *J. Mater. Chem.*, 2011, **21**, 7326.

29 C. I. Cámara, C. A. Bornancini, J. L. Cabrera, M. G. Ortega and L. M. Yudi, *Talanta*, 2010, **83**, 623–630.

30 R. P. Buck and E. Lindner, *Acc. Chem. Res.*, 1998, **31**, 257.

31 J. S. Río, O. Y. F. Henry, P. Jolly and D. E. Ingber, *Nat. Nanotechnol.*, 2019, **14**, 1143–1149.

32 S. S. Timilsina, P. Jolly, N. Durr, M. Yafia and D. E. Ingber, *Acc. Chem. Res.*, 2021, **18**, 3529–3539.

33 M. Karaboğ and M. K. Sezgintürk, *J. Pharm. Biomed. Anal.*, 2022, **209**, 114479.

34 Y. Liu, Z. Liu, F. Zhao and Y. Tian, *Angew. Chem., Int. Ed.*, 2021, **60**, 14429–14437.

35 C. Zhang, Z. Liu, L. Zhang, A. Zhu, F. Liao, J. Wan, J. Zhou and Y. Tian, *Angew. Chem., Int. Ed.*, 2020, **59**, 20499–20507.

36 L. Liu, F. Zhao, W. Liu, T. Zhu, J. Zhang, C. Chen, Z. Dai, H. Peng, J. Huang, Q. Hu, W. Bu and Y. Tian, *Angew. Chem., Int. Ed.*, 2017, **56**, 10471–10475.

37 T. Feng, W. Ji, Y. Zhang, F. Wu, Q. Tang, H. Wei, L. Mao and M. Zhang, *Angew. Chem., Int. Ed.*, 2020, **59**, 23445–23449.

38 A. Golabchi, B. Wu, B. Cao, C. J. Bettinger and X. T. Cui, *Biomaterials*, 2019, **225**, 119519.

39 M. Douglas, D. Rizzolo and D. Kruger, *Clin. Rev.*, 2017, **27**, 40–49.

40 A. F. Andrew, C. T. Robert, Y. G. Eugene and A. F. Robert, *World Neurosurg.*, 2016, **88**, 32–35.

41 R. Rasmussen, E. Nicholas, N. C. Petersen, A. G. Dietz, Q. Xu, Q. Sun and M. Nedergaard, *Cell Rep.*, 2019, **28**, 1182–1194.

42 H. Monai, S. Koketsu, Y. Shinohara, T. Ueki, P. Kusk, N. L. Hauglund and A. J. Samson, *Sci. Rep.*, 2021, **11**, 8150.

43 W. Stummer, A. L. Betz and R. F. Keep, *J. Cereb. Blood Flow Metab.*, 1995, **15**, 336–344.